Analysis of Dynamic Spatiotemporal Changes in Actual Evapotranspiration and Its Associated Factors in the Pearl River Basin Based on MOD16

Tao Zhang [iD] and Yangbo Chen *

School of Geography and Planning, Sun Yat-Sen University, Guangzhou 510275, China;
zhangt239@mail2.sysu.edu.cn
* Correspondence: eescyb@mail.sysu.edu.cn; Tel.: +86-208-411-4269

Abstract: Evapotranspiration is an important part of the hydrological cycle, surface energy balance and global climate system. Due to spatial heterogeneity, the trends in actual evapotranspiration (ET) and its associated factors vary in different regions. Because direct measurements of ET are limited over large areas, remote sensing provides an efficient method of ET spatial analysis, and standard data products are available at the global scale. This study uses the monthly MOD16 ET dataset and daily meteorological data to analyze the dynamic spatiotemporal changes in ET and its associated factors in the Pearl River Basin (PRB) from 2000 to 2014. The results of the study are as follows. (1) Over time and space, annual ET exhibited a slight increasing trend from 2000 to 2014, with an average value of approximately 946.56 mm/a. ET considerably varied at the monthly and seasonal scales, and in July displayed the highest monthly ET of approximately 119.57 mm, accounting for 36.37% of the annual ET. (2) ET displayed obvious spatial heterogeneity. Specifically, the west was a low-ET region, and moderate and high ET values were interspersed in the central and eastern PRB. Moreover, the rate of change of ET ranged from −13.99 mm/a to 12.81 mm/a in space, and 46.25% of the basin exhibited an increasing trend. (3) Dynamic changes in ET were mainly associated with temperature and relative humidity (RH). Additionally, energy-related elements and wind speed were positively correlated with ET, and temperature was the most influential factor of ET in some months (February–March and September–November). RH was the most important factor in other months but negatively correlated with ET in June and July. Affected by the actual environmental condition, qualitative changes were observed in the correlation between RH and ET in different months. The positive and negative spatial correlations between ET and its associated factors changed in different regions and in different months, and the changes mainly occurred from northwest to southwest.

Keywords: evapotranspiration; spatiotemporal; meteorological factor; MOD16; Pearl River Basin

1. Introduction

Evapotranspiration (ET), including evaporation from the soil and water surface and the transpiration of water through plant stomata, is a process of water conveyance from the underlying surface to the atmosphere [1–4]. ET transmits 62% of the precipitation back to the atmosphere and with precipitation, it can be used to assess regional wet and dry conditions [5]. Additionally, ET significantly influences the land surface water balance. Notably, 60% of the radiation energy at the surface is associated with ET, which is the main component of the regional surface energy, climate system and water cycle [6]. Moreover, ET is a key factor used to estimate the amount of the water available for ecological processes and agricultural irrigation [7]. Research on ET changes and responses to climate change can improve the understanding of water cycle and energy balance processes, and an

important content of water cycle, agricultural irrigation and climate change research under different global change scenarios [8–11].

Because of the importance of ET, researchers around the world have extensively investigated ET changes [8,12–16]. Generally, ET trends should increase in the context of global warming; however, observations have shown that actual ET and pan ET have decreased, and this contrary phenomenon is called the evaporation paradox [17]. Study showed the reference ET decreased in China in all seasons from 1954 to 1993, with increases in the northeast and southwest and decreasing trends in the northwest and southeast [8]. Another study showed annual ET exhibited a decreasing trend in most areas east of 100° E in China from 1960 to 2002 and an increasing trend in the western and northern parts of northeast China [18]. Cong suggested that pan ET in China decreased from 1956 to 1985 and increased from 1986 to 2005 [19]. But reference evapotranspiration also showed increasing trend in some regions such as in southern Iran, Spain, Poland, and the Loess Plateau in China [20–23]. These results suggest that ET in different regions exhibits different trends.

Moreover, the main factors associated with ET will change due to the heterogeneity of different regions [11,13,24–27]. Gong et al. suggested the humidity was the main factor that influenced reference ET in the Yangtze River Basin [28]. Yang et al. postulated that radiation and wind speed were the main factors associated with pan evaporation in China [29]. Another study found that relativity humidity, temperature, shortwave radiation and wind speed were the main factors that affected reference ET in the Hai River Basin [30]. Radiation was the most factor that most influenced the annual reference ET in the West Liao River Basin, while the average temperature, maximum temperature and relative humidity were the main factors in different seasons [26]. The response of ET to climate change varies in different regions and at different time scales; therefore, extensive research is required to investigate the factors related to ET in different regions and at different time scales [13,31–33].

Researchers have used many methods to estimate ET in different regions [34–36]. Traditional methods rely on observation data from pan ET, energy balance Bowen ratio systems, eddy covariance measurements, large aperture scintillators, the crop factor method or ET calculation formulas [2,12,37–40]. Although using the metrological data and interpolation methods can give a long-term ET, affected by the number, spatial distribution, and heterogeneity of observation stations, the regional accuracy of high-resolution spatial ET is difficult to assess [41,42]. With the development of new technologies, remote sensing can cover extensive regions and provide high-resolution information [43–46]. Based on the Landsat, Advanced Very High Resolution Radiometer, Moderate Resolution Imaging Spectroradiometer (MODIS) and other types of remote sensing images, the surface energy balance model, temperature plant index, and other estimation methods have been developed [43,47,48], these can give a high-resolution ET spatial change in a large region.

Based on the Penman–Monteith model, Mu used MODIS data and meteorological data to produce the official ET product of the National Aeronautics and Space Administration (NASA): MOD16 ET [49,50]. This dataset provides eight-day, monthly and annual intervals of ET for global vegetated land areas at a 1-km^2 resolution, and reliable data can be conveniently obtained free of charge for ET studies in different region of the world [10,51]. Numerous researchers have used these data for studies in different regions [52,53]. Notably, the MOD16 ET dataset performs well in forest areas and can estimate ET with reasonable accuracy [54]. Additionally, the MOD16 ET dataset perform best in studies of sites located in temperate and humid climates [10]. Wu et al. used the MOD16 ET to study the characteristics of land surface ET in the Poyang Lake Basin [55]; He et al. investigated surface ET in Shanxi Province based on the MOD16 product [56]; and Li et al. used the MOD16 ET to analyze the drought condition in Hainan Province [57]. Overall, based on the MOD16 product, many ET studies have been completed in the midwestern region of China, but few studies have been conducted in southern China.

The Pearl River is the third largest river and with the second highest flow in China. Due to its location in a region of land and sea intersection in Southeast Asia, it is impacted by the South China Sea monsoon and tropical cyclones. Additionally, the basin receives considerable rainfall with an uneven

spatial distribution. Although basin rainfall has increased in the past half century, accompanied by increased temperatures and ET changes, drought has occurred, resulting in complex changes in the hydrological regime of the basin [58,59]. The hydrologic process in the Pearl River and its tributaries has a major influence on the Pearl River Delta region downstream, and one tributary—Dongjiang River—is the drinking water source for Shenzhen City and Hong Kong. Notably, 80% of Hong Kong's drinking water comes from the Dongjiang River [60]. Moreover, the Pearl River Delta region is an important economic development zone that accounts for almost 10% of the Chinese Gross Domestic Product (GDP). Therefore, research on the dynamic spatiotemporal changes in ET and the associated influential factors in the Pearl River Basin (PRB) is important and of practical significance for socioeconomic development, water security and agriculture safety in the basin. Such information provides a reference for studies of hydrological scenarios and changes in flood and water resources in a low latitude sea-land interchange zone in the context of global warming [61,62].

Water cycle in the PRB had significant meanings in south China and gives reference information for the water cycle research in the PRB. So, based on the MOD16 ET dataset and daily meteorological data, this study investigated the dynamic spatiotemporal changes in ET in the PRB at the annual and monthly scales, the relationship between ET and its influential factors from 2000 to 2014.

2. Materials and Methods

2.1. Study Area

The PRB is located in southern China between 102°14′ E and 115°53′ E, 21°31′ N and 27°0′ N, and it includes parts of Yunan Province, Guizhou Province, Guangxi Province, Guangdong Province, Hunan Province, Jiangxi Province and Vietnam. The maximum elevation in the basin is approximately 2933 m, and the basin area is approximately 45.57×10^4 km^2. Additionally, the main tributaries include the Xijiang River, Beijiang River and Dongjiang River (Figure 1). The basin terrain is complex, with elevation gradually increasing from east to west. The southeastern region is a coastal area, and the northern region is mountainous. Western is the Yunan–Guizhou Plateau. The basin is mainly divided into three parts from west to east: the Yunan–Guizhou Plateau, the Guangdong, Guaongxi hills and the Pearl River Delta. The PRB is located in tropical and subtropical monsoon climate zones. Specifically, the multiannual average temperature varies between 14 and 22 °C, and the annual average precipitation is approximately 1525.10 mm and concentrated between April and September, when 80% of the annual precipitation occurs [63].
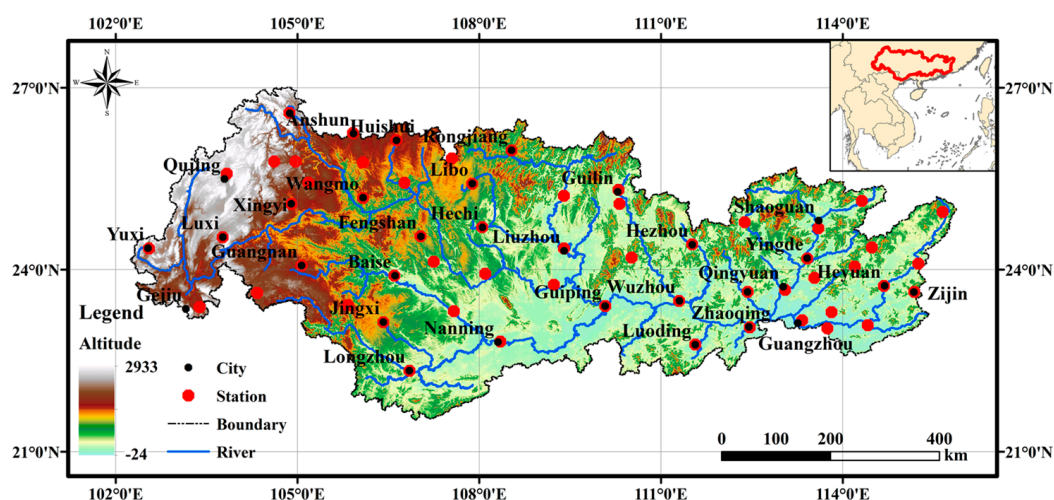

Figure 1. Location of the study area.

2.2. Data

Study data include regional monthly MOD16 ET data and daily meteorological data from 2000 to 2014.

ET data were from the monthly MOD16 ET dataset (1KM resolution) obtained from the Numerical Terra Dynamic Simulation Group website (http://www.ntsg.umt.edu/project/mod16). This dataset provides global surface ET estimates based on MODIS remote sensing data and meteorological data.

There are 114 meteorological stations in and around the basin. All of the meteorological data were acquired from China's ground climatological daily dataset (V3.0) provided by the China National Meteorological Information Center (http://data.cma.cn/). After the data were assessed, stations with missing data for more than 60 continuous days were eliminated. Thus, this study used high-quality meteorological data from 57 meteorological stations in the basin and 43 stations near the basin. These 100 stations provided data for six meteorological elements at the daily scale. These elements include daily maximum temperature (T_{max}), average temperature (T_{avg}), daily minimum temperature (T_{min}), wind speed (V), relative humidity (RH) and sunshine hours (n). Anomalous values were corrected based on the data from adjacent days, and this process does not influence trends in long-term meteorological data.

Regional runoff data using the statistical data in the PRB water resource report released by the Pearl River Water Resources Commission of the Ministry of Water Resources, China (http://www.pearlwater.gov.cn/xxcx/szygg/).

2.3. Analysis Method

2.3.1. Data Processing

To research the spatial correlation between ET and its associated factors, the spatial distributions of meteorological variables should be determined. Kriging and Inverse Distance Weighted (IDW) are popular spatial interpolation methods that have been used in many studies [64]. We selected ordinary kriging with spherical variogram (Ks), ordinary kriging with exponential variograms (Ke), universal kriging with linear drift variograms (Kl) and IDW to analyze the monthly interpolation results of T_{max}, T_{avg}, T_{min} and RH in ArcGIS software. We choose 60 stations for interpolation, and the other 40 stations were used to verify the interpolation results.

Then, we used SPSS software to complete the correlation calculations between interpolated and observed values of T_{max}, T_{avg}, T_{min} and RH at the 40 stations in one random month of each year from 2000 to 2014. The results indicated that Ks provided the highest correlation coefficient values (Table 1). Therefore, we chose Ks to interpolate the monthly T_{min} and RH values from the 100 stations. Finally, we produced the regional monthly spatial distributions of T_{min} and RH at a 1-km grid resolution, which is the same spatial resolution as MOD16 ET, from 2000 to 2014 in the PRB. And, in this article, all of the average values of different elements were an arithmetical mean from the all grids (1 km resolution) of the whole basin.

Table 1. Correlation coefficients between the interpolation results and observed data.

| Methods Factors	Ks	Ke	Kl	IDW
T_{max}	0.999	0.985	0.983	0.984
T_{avg}	1.000	0.986	0.986	0.986
T_{min}	1.000	0.987	0.986	0.986
RH	0.976	0.848	0.848	0.839

2.3.2. Data Verification

The study extracted the monthly ET in PRB from 2000 to 2014 based on the MOD16. In order to ensure the accuracy and correct of the data, this article using the water balance method to test its effectiveness, obtained the regional ET change data by the regional water balance.

$$Q = P - \text{ET} \times A - \Delta S \tag{1}$$

Q—runoff ($10^9 \times$ m^3); P—regional precipitation ($10^9 \times$ m^3); A—basin area (km^2); ΔS—dynamic change of the regional store water, mainly the ground water and lake, ignore under the annual scale situation. After verification, the correlation between calculate Q (Q_{calc}) and observation Q (Q_{ob}) about 0.89 (Figure 2), these data had a high consistency, verified the ET can meet the needs of the ET spatial-temporal distribution research in PRB.
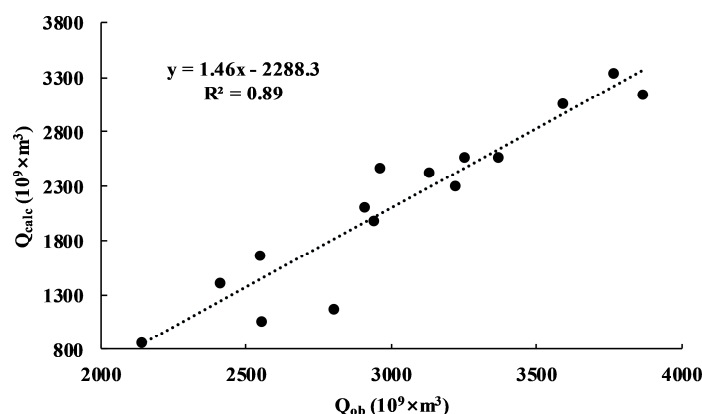
Figure 2. Relation between observed runoff Q_{ob} and runoff calculated from water balance equation Q_{calc}.

2.3.3. Trend Analysis

MOD16 ET was used to produce a spatial ET distribution, and each pixel was based on 15 years of data from 2000 to 2014. Using Sen's slope (2) and the pixel values in each year, the 15-year accuracy change trend value in each pixel (1 km $\times$ 1 km) in the PRB was calculated in ArcGIS software. In addition, the trend in each pixel was combined to determine the overall spatial ET trend in the PRB. The aforementioned equation is as follows [65]:

$$\text{SLOPE} = \frac{N \times \sum\limits_{k=1}^{N} k \times \text{ET}_k - \sum\limits_{k=1}^{N} k \sum\limits_{k=1}^{N} \text{ET}_k}{N \times \sum\limits_{k=1}^{N} k^2 - (\sum\limits_{k=1}^{N} k)^2} \tag{2}$$

where N is the research period (15 years from 2000 to 2014), k is the year number (1 through 15), and ET_k is the ET value of a pixel in year k. If the slope is greater than 0, ET increases in the pixel, and a slope less than 0 reflect the opposing trend. Sen's slope also using for the trend detection of different associated factors.

Nonparametric statistical analyses, the Mann–Kendall (MK) trend test was used to detect the temporal significant ET changes, and using Python and ArcGIS soft completed the significant test of each grid. MK has been widely used to access the significance of trends in hydro-meteorological time series [20]. The Mann–Kendall test was calculated as follows Equations (3)–(6) [20,66,67]:

$$S = \sum_{k=1}^{N-1} \sum_{j=k+1}^{N} \text{sign}(x_j - x_k) \tag{3}$$

$$\text{sign}(x_j - x_k) = \begin{cases} 1 & (x_j - x_k) > 0 \\ 0 & (x_j - x_k) = 0 \\ -1 & (x_j - x_k) < 0 \end{cases} \tag{4}$$

$$\text{Var}(S) = \left\{ [N(N-1)(2N+5)] - \sum_{i=1}^{m} t_i(t_i - 1)(2t_i + 5) \right\} / 18 \tag{5}$$

$$Z = \begin{cases} (S-1)/\sqrt{\text{Var}(S)} & S > 0 \\ 0 & S = 0 \\ (S+1)/\sqrt{\text{Var}(S)} & S < 0 \end{cases} \tag{6}$$

N is the number of each grid's data—it's the research period (15 years from 2000 to 2014) in this article. x_j and x_k are the sequential data values of each grid; t_i is the number of ties of extent m. Z is the standardized Mann–Kendall statistics. Positive values of Z indicate increasing trends, while negative values of Z show decreasing trends. When $|Z| \geq Z_{1-\alpha/2}$, the null hypothesis was rejected. We set significance levels at $\alpha = 0.01, 0.05$ and 0.1.

2.3.4. Correlation Analysis

First, the temporal correlation between annual ET and its meteorological factors was analyzed in SPSS software based on the annual average ET and meteorological factors at the basin scale.

Second, spatial correlation between ET and meteorological factors was performed to discuss the dynamic spatiotemporal changes in ET in the PRB due to different meteorological factors. This study used the correlation coefficient calculation shown in Formula (7) completed the spatial correlation analysis of ET and meteorological factors at the pixel scale using ArcGIS software [68]:

$$R_{xy} = \frac{\sum\limits_{k=1}^{N} \left[(x_k - \bar{x})(\text{ET}_k - \overline{\text{ET}}) \right]}{\sqrt{\sum\limits_{k=1}^{N} (x_k - \bar{x})^2 \sum\limits_{k=1}^{N} (\text{ET}_k - \overline{\text{ET}})^2}} \tag{7}$$

where R_{xy} is the correlation coefficient of the two variables (x and y); N is the length of the research period (15 years from 2000 to 2014); k is the year number (1 through 15); x is the raster-based interpolation result of the monthly meteorological variable (e.g., T_{min}, RH, etc.); y is the raster-based monthly ET in the PRB; $\bar{x}$ and $\overline{\text{ET}}$ are the raster-based monthly averaged interpolation results of meteorological factors and ET in the PRB for each pixel.

3. Results

3.1. Temporal Change in Evapotranspiration (ET) in the Pearl River Basin (PRB)

Figure 3 shows the fluctuation in annual ET from 2000 to 2014. Notably, ET varies from 925.19 mm to 987.71 mm, a slight increasing trend, with an annual average of 946.56 mm/a. ET was low between 2000 and 2002 and dramatically increased in 2003 to a maximum value of approximately 987.71 mm. Then, ET decreased after 2007, with a minimum of approximately 925.19 mm in 2010. 2007 and 2013 were years with high values, with a slight decrease in 2014. Although ET exhibited many rapid changes during the study period, the overall floating range does not exceed 5% of the mean annual ET.
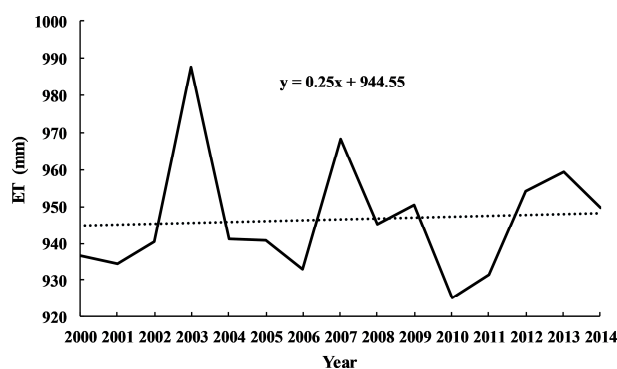
Figure 3. Variation in annual evapotranspiration (ET) in the Pearl River Basin (PRB) from 2000 to 2014.

Seasonal ET variations are shown in Figure 4. Spring and winter ET displayed slight decreasing trends, while summer and autumn ET exhibited slight increasing trends. Spring ET exhibited an increasing trend from 2000 to 2003, with a maximum in 2003 of approximately 251.67 mm, exceeding the average by 7.65%. The minimum spring ET of approximately 217.42 mm occurred in 2011. The summer ET trend differed from the spring ET trend with considerable variation. The first low value in 2001 was approximately 332.30 mm, which was 96.53% of the average value. Then, the summer ET increased to a maximum of 362.39 mm in 2007 before decreasing to a minimum of approximately 329.01 mm in 2014. The autumn ET exhibited an obvious increasing trend, changing from 233.48 mm to 257.22 mm between 2000 and 2005. After 2005, ET decreased, with a low value of approximately 238.75 mm in 2010. Then, autumn ET increased to 255.91 mm in 2014. Winter ET exhibited a decreasing trend with large fluctuations, including a peak value of approximately 129.23 mm in 2003 and a minimum value of approximately 112.65 mm in 2008.
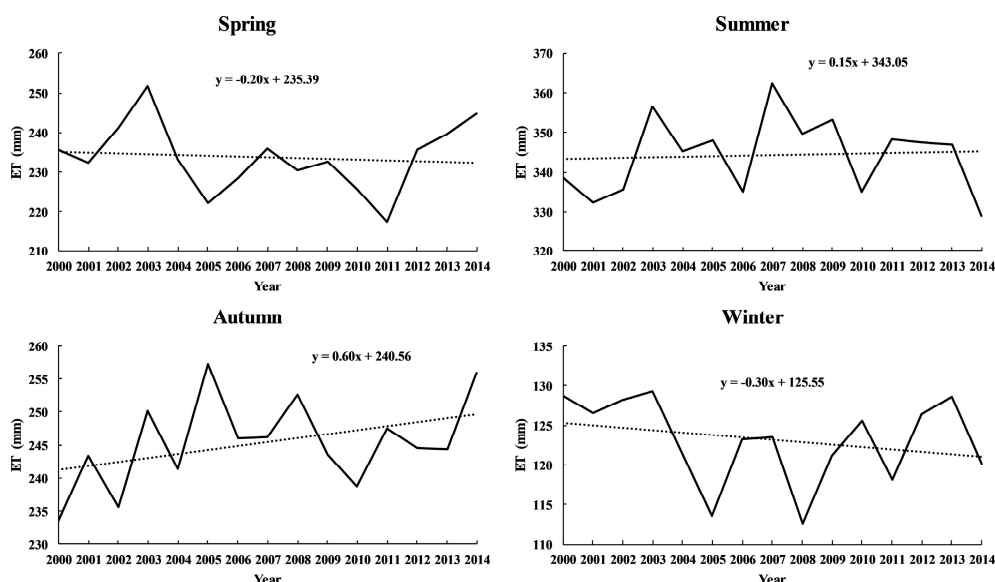
Figure 4. Variation in seasonal ET in the PRB.

The distribution of monthly ET in the PRB has a certain regularity change (Table 2), increasing from January to July and decreasing after July. January exhibited the lowest ET of approximately 39.05 mm, and the highest ET of approximately 119.57 mm occurred in July. Additionally, ET is greater than 100 mm from June to September and decreases to 39.37 mm in December. Seasonally, the average ET is approximately 233.79 mm, 344.25 mm, 245.38 mm, 123.12 mm in spring (March–May), summer

(June–August), autumn (September–November) and winter (December–February), respectively. Summer had the highest seasonal ET, more than 2.80 times that in winter and 36.37% of the yearly ET.

Table 2. Monthly variation in ET in the PRB (mm).

Month	1	2	3	4	5	6	7	8	9	10	11	12
ET	39.05	44.71	59.95	76.00	97.84	107.85	119.57	116.82	106.34	84.36	54.68	39.37

3.2. Spatial Distribution of the ET in the PRB

The spatial change in ET in the PRB exhibited significant spatial heterogeneity (Figure 5). Specifically, the western region was mainly characterized by low ET, and the distributions in the central and eastern regions were characterized by moderate and high values. Because no ET data were available for water and building areas in the MODIS data series, these areas are denoted as "No data" in this study and account for 1.57% of the basin. In addition, ET in the PRB was divided into four intervals: 338.27–700 mm, 700–900 mm, 900–1100 mm and 1100–1665.10 mm.
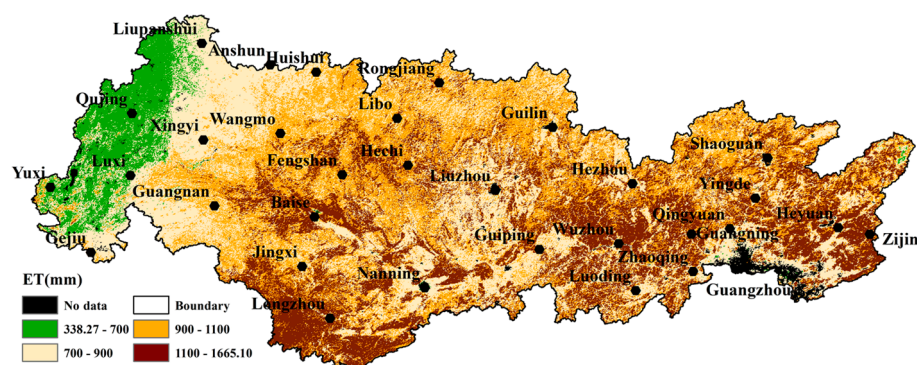
Figure 5. Spatial distribution of the ET in the PRB.

The 338.27–700 mm class was mainly distributed in the high-elevation region between Gejiu and Liupanshui and accounted for approximately 6.66% of the total basin area. The second interval (700–900 mm) accounted for approximately 35.98% of the total basin area and was distributed in the west of Wangmo, the central region around Guiping and Liuzhou and Pearl River Delta. Additionally, the 900–1100 mm class accounted for a large proportion of approximately 29.62% of the basin and exhibited a distribution around the second interval region. In addition, 26.17% of the basin was classified as 1100–1665.10 mm of ET, with the highest value mainly distributed near Longhzou, Baise, Wuzhou and Heyuan.

Monthly ET exhibited obvious spatial change. As shown in Figure 6, ET was low from January to March at mainly under 60 mm. However, ET was approximately 90 mm near Longzhou, Nanning, Wuzhou and Heyuan and gradually increased from south to north. In April, a new region of high ET was observed near Fengshan in the central portion of the region based on the previous distribution pattern. From May to September, the lowest ET values were observed west of Gejiu, Guangnan and Huishui. In the remainder of the region, ET averaged approximately 120 mm, and the highest monthly ET was approximately 206.95 mm. The central area, including Nanning, Liuzhou and Guiping, exhibited moderate values. ET decreased from the north to south from October to December, and the areas near Longzhou, Wuzhou and Heyuan exhibited the slowest decreases and had the highest ET values. The high-elevation western region displayed the lowest ET in each month.
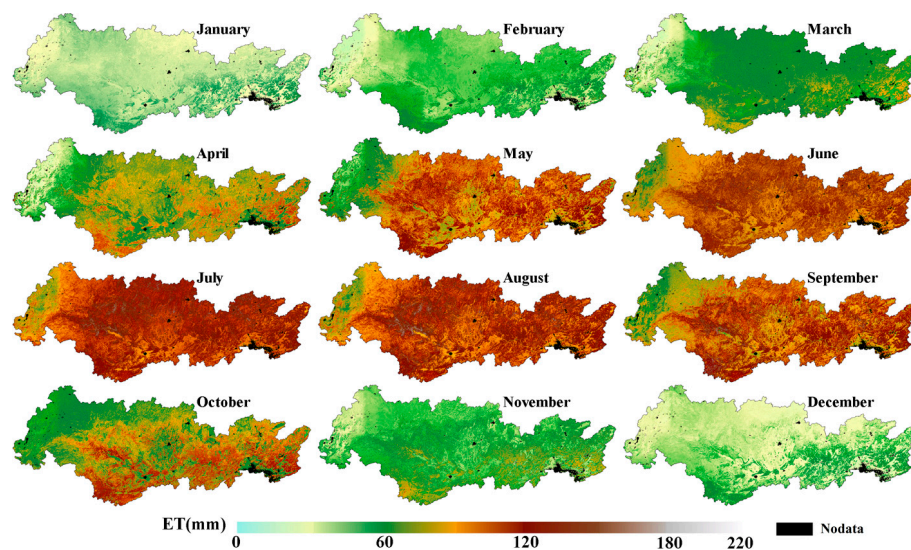
**Figure 6.** Spatial variation in monthly ET in the PRB.

3.3. Spatial Change Trend in ET in the PRB

The annual spatial change in ET was calculated from 2000 to 2014 at the pixel scale using ArcGIS (Figure 7). Notably, 53.75% of the basin exhibited a decreasing trend. Decreasing trends were observed west of Gejiu and Liupanshui in the western basin, near Baise and Naning in the southwestern region, and north of Liuzhou, Qingyuan and Shaoguan. The highest decreasing rate was approximately 13.39 mm/a. Conversely, 46.25% of the region displayed an increasing trend, with the highest increasing rate of approximately 12.81 mm/a.

Seasonal ET exhibited different spatial changes in the PRB (Figure 7). Slope trend result showed the rate of change of spring ET varied from −3.50 mm/a to 3.23 mm/a, and most regions exhibited decreasing trends. Specifically, only 39.02% of the study area exhibited an increasing trend, and these increases were mainly distributed to the west of Hechi, Wuzhou and Heyuan. The rate of change of summer ET varied from −5.03 mm/a to 4.73 mm/a, and 54.17% of the basin exhibited an increasing trend. The rate of change of autumn ET ranged from −5.12 mm/a to 3.56 mm/a, with increasing trends in approximately 64.95% of the basin. Winter ET exhibited a small change ranging from −2.48 mm/a to 2.12 mm/a, and only 27.07% of the basin exhibited an increasing trend. These increases were mainly distributed to the east of Anshun, north of Xingyi and Hechi, and south of Guangnan, as well as in the Pearl River Delta area.

The MK test showed almost 90% region of the basin had no significance change in yearly and seasonal ET. There only have 0.88% region showed significance decreasing, 0.83% region showed increasing change in 0.01 level of the yearly ET change trend; 2% and 3.14% in 0.05 level. Seasonal ET change, decreasing or increasing trend in 0.01 significance level all distributed less than the 1% region, excluding the 3.47% region, which showed an increasing trend in winter. The 7.17% region, which is mainly distributed in the middle region of the basin, showed an increasing trend in 0.05 significance level in winter, with less than the 4% region in other seasons showed decreasing or increasing trend in 0.05 significance level.
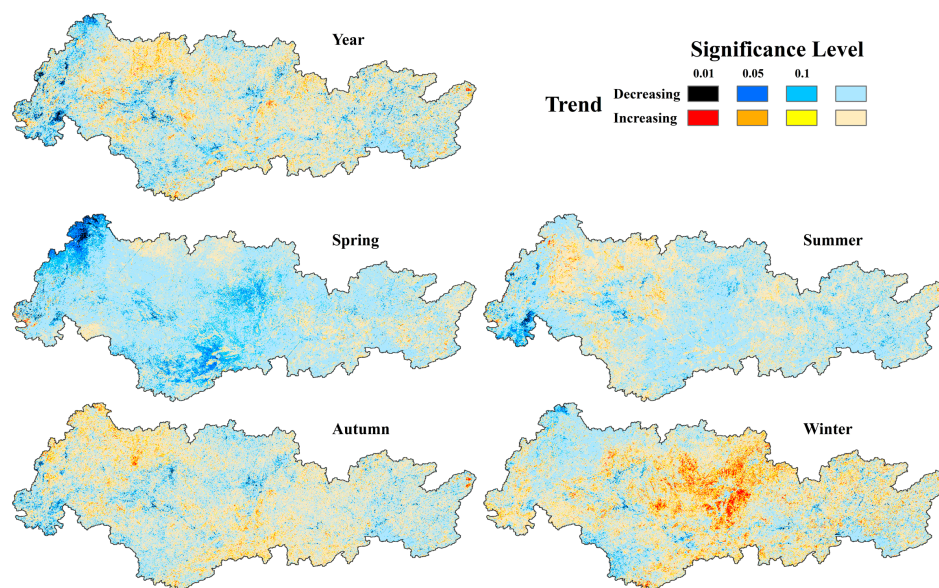
Figure 7. Spatiotemporal changes and significance level in yearly and seasonal ET in the PRB.

3.4. ET Factors in the PRB

ET is the product of the collective effects of regional surface environment conditions and climatic conditions. In this study, six factors were selected to discuss the effects of meteorological factors on ET. The results showed that meteorological factors have different change trends and different influences on ET changes in different months (Table 3). Temperature showed an increasing trend except for in winter; RH decreased for almost the whole year; V showed an increasing trend during the whole year; n showed an increase in the summer. The energy-related elements, such as temperature and sunshine hours, had the largest effects on ET from February to April and from August to October. Additionally, meteorological factors did not significantly influence ET in May; RH had the most notable influence on ET from June to July, exhibiting a very significant negative correlation. The effects of energy-related elements on ET gradually decreased from November to January; RH exhibited an increasing effect on ET, and exhibited very significant positive correlations with ET. V and n had significant effects on ET in January, June and July, respectively. The effect of RH on ET considerably varied, with a positive correlation from February to May, negative correlation from June to October, very significant negative correlation in June and July, and a very significant positive correlation from November to January.

The changes in monthly ET and the correlations between ET and different factors suggest that temperature was the main factor that influenced ET from February to May and September to November. Moreover, T_{min} had the highest correlation coefficient, and RH exhibited a high correlation coefficient with ET. Therefore, T_{min} and RH are chosen as the meteorological factors that indicate ET spatial changes, and a pixel-scale analysis of spatial changes in the correlation coefficient was performed.

The correlation coefficient between ET and T_{min} exhibited obvious spatial changes (Figure 8). In spring, a negative correlation region can be initially observed in the western region, and it then expands to the east and from north to south. In summer, the negative correlation region reaches its largest extent, with low correlation coefficients mainly distributed in the southern portion of the region. Moreover, the negative correlation region retreated to the north and west from the south in July. In autumn, positive correlations exhibited an increased distribution, and the correlation coefficient exhibited an increasing trend. Positive correlations were distributed throughout the basin in October and November, and the associated correlation coefficients were high. In winter, the negative correlation region appeared in the northwest and expanded.

Table 3. Meteorological factors trend (T) and correlation coefficients (R) with ET in the PRB.

Factors	T_{max}		T_{avg}		T_{min}		RH		V		n	
Month	T	R	T	R	T	R	T	R	T	R	T	R
January	−0.79	0.16	−1.48	0.30	−1.58	0.60 *	−0.99	0.70 **	0.20	0.65 **	−0.89	0.52 *
February	0.40	0.73 **	0.20	0.77 **	0.00	0.79 **	−1.58	0.24	1.68	−0.05	0.40	0.48
March	0.10	0.49	0.00	0.62 *	−0.20	0.72 **	−1.48	0.43	1.09	−0.01	0.00	0.32
April	−0.49	0.50	−0.40	0.63 *	0.10	0.73 **	−0.20	0.21	0.40	0.51	−0.79	0.28
May	0.20	0.16	0.30	0.25	0.59	0.30	0.00	0.35	2.38	−0.05	−0.79	−0.16
June	0.89	0.53 *	0.79	0.35	1.09	−0.04	−0.79	−0.64 **	1.39	0.22	−0.69	0.71 **
July	0.59	0.45	0.40	0.50	1.39	0.40	−0.79	−0.66 **	2.08	0.46	0.20	0.45
August	1.58	0.50	0.99	0.52 *	0.10	0.52 *	−2.38	−0.50	3.17	0.22	1.48	0.22
September	0.69	0.64 *	0.79	0.67 **	1.68	0.67 **	0.30	−0.06	2.97	−0.02	0.10	0.26
October	1.09	0.80 **	0.30	0.79 **	0.00	0.66 **	−1.78	−0.10	1.09	−0.34	1.48	0.20
November	−0.40	0.60 *	1.19	0.87 **	1.78	0.90 **	0.79	0.72 **	1.39	−0.24	−1.09	−0.40
December	−1.58	0.35	−1.48	0.61 *	−0.89	0.69 **	−1.29	0.88 **	1.29	0.02	−0.30	−0.37

Notes: ** indicates significance at the 0.01 probability level; * indicates significance at the 0.05 probability level; T_{max}: maximum temperature; T_{avg}: average temperature; T_{min}: minimum temperature; RH: relative humidity; V: wind speed; n: sunshine hours.
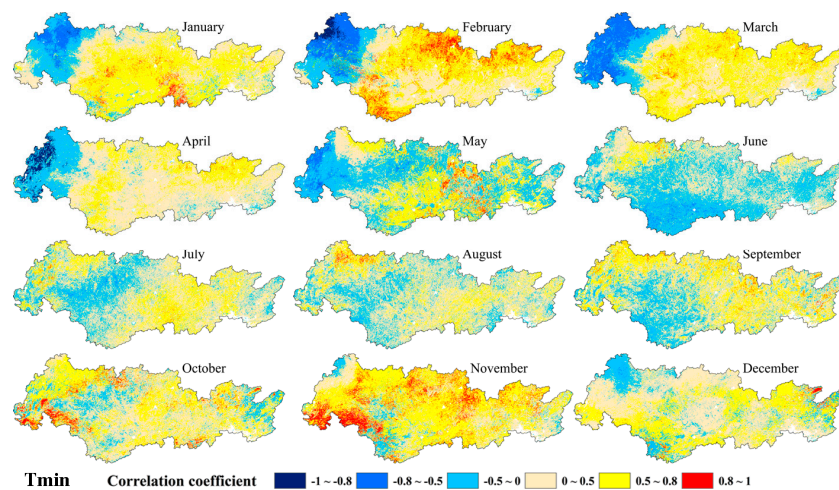
Figure 8. Spatial distribution of the correlation coefficient between ET and daily minimum temperature (T_{min}) in the PRB.

The correlation between RH and ET exhibited obvious spatiotemporal variation and a slight contrast to the T_{min} distribution (Figure 9). The positive correlation region gradually shrank from east to south, and the negative correlation region expanded from north to south in spring. In summer, negative correlations were distributed throughout the basin, excluding the high-elevation western region. In autumn, the positive correlation region expanded to Nanning, Liuzhou and Guiping in the central region, and positive correlations were mainly observed in the western portion of the basin in November. Most regions in the basin displayed positive correlations in winter, and the region with the highest positive correlation coefficient shifted from east to west. Overall, positive correlations were mainly distributed in the west, and the negative correlation region expanded from east to northwest, with the broadest distribution in July. Then, positive correlations expanded from the west, the negative correlation region shrank.
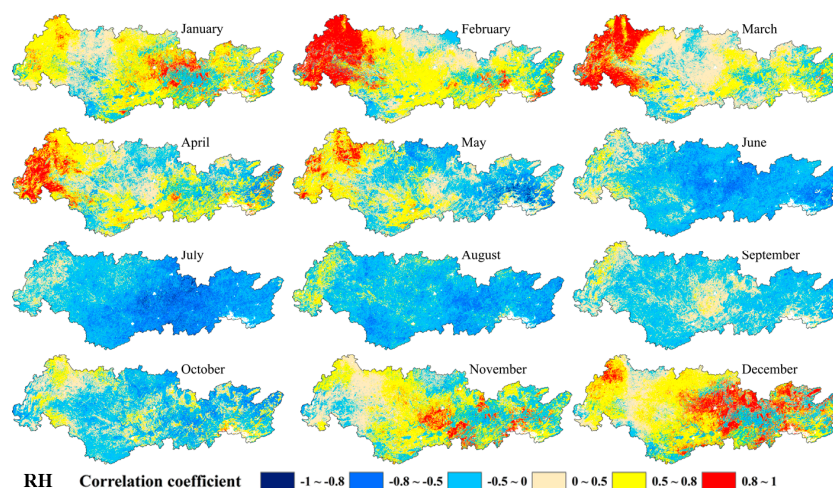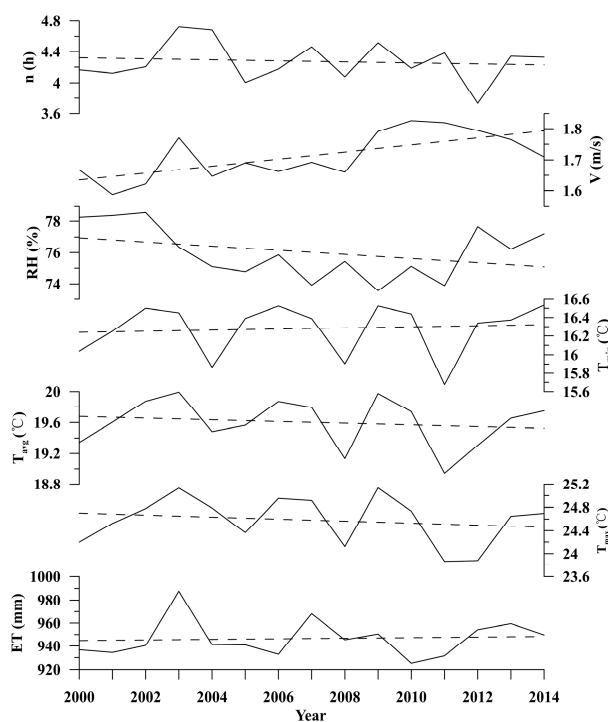
Figure 9. Spatial distribution of the correlation coefficient between ET and relative humidity (RH) in the PRB.

4. Discussion

4.1. Analysis of Temporal Changes in ET

Based on the MOD16 ET dataset, we analyzed the correlation between ET and its associated factors in the PRB from 2000 to 2014, as shown in Figure 10.

Figure 10. Dynamic changes in ET and its associated meteorological factors in the PRB.

ET was stable at the start of the study period and then rapidly increased from 2000 to 2003. T_{max}, T_{avg} and T_{min} displayed stable increasing trends from 2000 to 2003; T_{avg} and n increased by 0.65 °C and 0.56 h, respectively. These results reflect an increase in the basin energy, which in turn increased ET. Additionally, V increased 0.18 m/s, got 1.77 mm/s in 2003 and was a driver of the ET increase. The increases in temperature and V, decrease in RH in 2003 significantly influenced ET from 2000 to 2003.

Then, a trough appeared from 2004 to 2006. In this period, T_{max} exhibited a continuous decreasing trend and reached a minimum in 2005. T_{avg} also exhibited a trough period, n and V decreased during this period. The decreases in n and temperature decreased the available energy in the basin, thereby reducing the ET capacity. The n in June and July in 2007 increased by 0.92 h and 0.6 h, respectively, and ET was highest in June and July. These increases in n increased the energy available for ET and caused ET to increase. From 2007 to 2011, the decreases in the temperature and energy caused ET to decrease. In addition, T_{max}, T_{avg} and T_{min} decreased to minimums in 2011 and caused ET to enter a trough period. The increase in ET from 2011 to 2014 exhibited a close relation with the temperature increase. Moreover, the decrease in V and increases in RH and p caused ET to decrease in 2014.

Overall, trends of ET result from the combined effects of different meteorological factors. During the study period from 2000 to 2014, the energy elements (T_{max}, T_{avg}, n) and RH exhibited decreasing trend while V increasing. V exhibited an increasing trend in the PRB from 2000 to 2014, which is consistent with previous research in Southwest China [69]. An analogous positive correlation between ET and V was also observed in the Changjiang catchment [64]. Slight increasing trends of ET were a combined result with increasing V and decreasing RH.

In addition, seasonal ET exhibited obvious changes and a close relation to climate in different months. The increases in radiation and temperature were driving forces of the spring ET increase. The temperature reached a maximum in summer, and the high radiation energy provided more energy for ET. Although, rainfall is mainly distributed in summer, the high summer temperatures lead to the highest seasonal ET. With the temperature decrease in autumn, ET also exhibited a decreasing trend. Winter displayed the lowest temperature, and energy limited the ET, resulting in the lowest seasonal ET. As well, the trend of each month ET was also the combined result of the change of the factors. Especially, the multiply result of trend of almost all factors and correlation coefficient gave a positive trend of the ET from April to September, then ET showed an increasing trend in summer and autumn from 2000 to 2014.

4.2. Analysis of the Spatial Distribution of ET

The underlying surface of the PRB is complex and diverse. The terrain is mainly divided into the Yunnan–Guizhou Plateau, the Guangdong–Guangxi hills and the Pearl River Delta. The weather is affected by the southwest monsoon and southeast monsoon, and the distribution of regional vegetation types is complicated [70]. The elevation in the west region is almost 3000 m, and the elevation is low in the east. These differences influenced the decreasing temperature trend from east to west and the significant reduction in energy sources. In addition, due to the high elevation in the west and lower vegetation cover than that in the east, the ET of vegetation in the western region is relatively low, and ET in the western region is lower than that in the eastern region. The low ET in Nanning, Liuzhou and Guiping are closely related to small areas of vegetation coverage and small distributions of forestland in the region [71]. The highest ET of greater than 1100 mm was mainly distributed in the southern region and near the equator. In these areas, ET exhibited close relations with n.

4.3. Analysis of the ET Factors

Based on the above analysis of the correlations between meteorological factors and ET in the PRB, temperature is the main factor that influences ET, but temperature is not always the most important factor in a given month or season. In spring, which is characterized by rising temperatures, ET increased, and the correlation coefficient exhibited an increasing trend. Although temperature increased, the temperature was relatively low, so ET was low. T_{min} has an important effect on the temperature threshold at which evaporation begins and the factors that influence ET. Therefore, T_{min} exhibited a very significant correlation with ET and was the most important factor that influenced ET. In addition, RH displayed positive correlation with ET along with the statics in the Haihe River Basin, Songnen Plain, Loess Plateau [72–74], and this result was different than those of other studies [15,75]. In summer, p increased and temperatures were high, but temperature and energy was the highest in

the year, and were not the limit factors of ET; the associated correlation coefficients exhibited decreasing trends. As p increased, RH also increased and reduces the pressure difference between the surface of the leaf and the atmosphere, had a negative effect on ET. Thus, RH and p were the controlling factors of ET. In autumn, as p and RH decreased, temperature became the main influential factor. Notably, temperatures remained high, and T_{avg}, rather than T_{min}, was the main controlling factor of ET. In addition, the temperature and RH decreased slower in the east than in the west, and the positive correlation between RH and ET increased from west to east. In winter, with the decreasing temperature trend, the importance of energy slightly declined, and the correlation with RH slightly increased. In addition, as T_{avg} increased in February, the correlation coefficient exhibited an increasing trend.

RH is a sensitive factor to ET [76]. Physically, RH had negative correlation with ET [40], especially with the reference and potential evapotranspiration [5,64,77,78]. In this study, the correlation coefficient between monthly RH and ET exhibited different quality correlations. It related to the water supply in different months. From the results from this study, we found RH had a negative correlation with ET from May to October. These months almost had 80% of the yearly precipitation [63]. The abundant precipitation caused high RH, made the air already close to saturation, and less additional water could be stored [40], so RH showed a negative correlation with ET. In the other months, lower precipitation caused lower water supply and lower RH; combined with the lower temperature in these months, ET showed a lower value. So, RH showed positive correlation with ET in statistics. The different water supply conditions in the region also cause the spatial distribution of a different quality correlation between RH and ET. The calculations of transpiration based on surface conductance in MOD16 ET and the correlation calculate by statistical also had an effect on the correlation. Positive correlations were also found between RH and ET in other regions [72–74]. Physically, RH had a negative correlation with ET, but in different regions; RH may show different quality correlation with ET under different actual environment water supply conditions. So, changes in correlation between variables including RH and ET require further research on the statistics result, physical basis and actual environment condition. The temporal correlations between ET and meteorological factors at annual and monthly scales and the spatial correlation at the pixel scale suggest that the changes in ET are closely related to climate change and significant impacted by spatial heterogeneity [64].

At the interannual scale, ET changes are typically affected by the energy terms, such as temperature and n. At the monthly scale, temperature, RH and n exhibited obvious effects on ET. The changes in ET and meteorological factors were obvious due to different climatic conditions in different months. The climatic conditions in different regions, which have unique spatial, elevation, latitude and terrain conditions, result in different controlling factors of ET in different regions at the same time. The spatial variations in influential factors and temporal changes in climatic conditions had different effects on ET based on different thresholds associated with different spatiotemporal conditions. Therefore, changes in ET over large, complex areas should be studied under different temporal and spatial conditions, and studies should focus on how changes in spatiotemporal factors influence ET [77].

5. Conclusions

Based on the MOD16 ET dataset, monthly ET data from the PRB, and meteorological data from 100 stations from 2000 to 2014, the spatiotemporal changes in ET and its associated factors were analyzed. The results indicate the following conclusions:

(1) ET fluctuated and slightly increased from 2000 to 2014, with a maximum of approximately 987.71 mm in 2003 and minimum of approximately 925.19 mm in 2010. Over time and space, annual ET averaged approximately 946.56 mm/a. ET exhibited slight decreasing trends in spring and winter and slight increasing trends in summer and autumn. Specifically, the maximum ET of approximately 344.25 mm occurred in summer, was 2.80 times the winter ET, and accounted 36.37% of the annual ET. Moreover, monthly ET displayed a certain regularity change.

(2) The spatial ET distribution in the PRB exhibited obvious spatial heterogeneity. Notably, the west was generally a low-value region, and the central and eastern regions exhibited a mix of moderate and high values. Longzhou, Baise, Wuzhou and Heyuan were the four centers of high ET. Additionally, annual ET varied from −13.9 mm/a to 12.81 mm/a, and 46.25% of the basin exhibited an increasing trend.

(3) The factors that influenced ET varied in different regions and at different times. Annual ET was mainly affected by the temperature, while monthly ET was mainly affected by the temperature (February–March and September–November) and RH. In addition, affected by the actual environmental condition, the quality of the correlation between RH and ET varied in different months and regions. The spatial variations in ET and its associated factors are affected by the complex effects of climatic conditions that vary at different elevations and latitudes and under different topographic conditions.

Author Contributions: Yangbo Chen conceptualized the study, and Tao Zhang was responsible for the data compilation, processing, illustrations and writing of the paper.

Conflicts of Interest: The authors declare no conflicts of interest.

References

1. Anderson, M.C.; Norman, J.M.; Mecikalski, J.R.; Otkin, J.A.; Kustas, W.P. A climatological study of evapotranspiration and moisture stress across the continental United States based on thermal remote sensing: 2. Surface moisture climatology. *J. Geophys. Res. Atmos.* **2007**, *112*. [CrossRef]
2. Allen, R.G.; Pereira, L.S.; Howell, T.A.; Jensen, M.E. Evapotranspiration information reporting: I. Factors governing measurement accuracy. *Agric. Water Manag.* **2011**, *98*, 899–920. [CrossRef]
3. Bisquert, M.; Sánchez, J.M.; López-Urrea, R.; Caselles, V. Estimating high resolution evapotranspiration from disaggregated thermal images. *Remote Sens. Environ.* **2016**, *187*, 423–433. [CrossRef]
4. Ma, Q.; Zhang, J.; Sun, C.; Guo, E.; Zhang, F.; Wang, M. Changes of reference evapotranspiration and its relationship to dry/wet conditions based on the aridity index in the Songnen Grassland, Northeast China. *Water (Switz.)* **2017**, *9*, 316. [CrossRef]
5. Guo, D.; Westra, S.; Maier, H.R. Sensitivity of potential evapotranspiration to changes in climate variables for different Australian climatic zones. *Hydrol. Earth Syst. Sci.* **2017**, *21*, 2107–2126. [CrossRef]
6. Katul, G.G.; Oren, R.; Manzoni, S.; Higgins, C.; Parlange, M.B. Evapotranspiration: A process driving mass transport and energy exchange in the soil-plant-atmosphere-climate system. *Rev. Geophys.* **2012**, *50*. [CrossRef]
7. Li, Z.L.; Tang, R.; Wan, Z.; Bi, Y.; Zhou, C.; Tang, B.; Yan, G.; Zhang, X. A review of current methodologies for regional evapotranspiration estimation from remotely sensed data. *Sensors* **2009**, *9*, 3801–3853. [CrossRef] [PubMed]
8. Thomas, A. Spatial and temporal characteristics of potential evapotranspiration trends over China. *Int. J. Climatol.* **2000**, *20*, 381–396. [CrossRef]
9. French, A.N.; Hunsaker, D.J.; Thorp, K.R. Remote sensing of evapotranspiration over cotton using the tseb and metric energy balance models. *Remote Sens. Environ.* **2015**, *158*, 281–294. [CrossRef]
10. Hu, G.; Jia, L.; Menenti, M. Comparison of mod16 and lsa-saf msg evapotranspiration products over Europe for 2011. *Remote Sens. Environ.* **2015**, *156*, 510–526. [CrossRef]
11. Zhang, D.; Liu, X.; Zhang, Q.; Liang, K.; Liu, C. Investigation of factors affecting intra-annual variability of evapotranspiration and streamflow under different climate conditions. *J. Hydrol.* **2016**, *543*, 759–769. [CrossRef]
12. Rana, G.; Katerji, N. Measurement and estimation of actual evapotranspiration in the field under Mediterranean Climate: A review. *Eur. J. Agron.* **2000**, *13*, 125–153. [CrossRef]

13. Roderick, M.L.; Rotstayn, L.D.; Farquhar, G.D.; Hobbins, M.T. On the attribution of changing pan evaporation. *Geophys. Res. Lett.* **2007**, *34*. [CrossRef]

14. Chen, Y.; Xia, J.; Liang, S.; Feng, J.; Fisher, J.B.; Li, X.; Li, X.; Liu, S.; Ma, Z.; Miyata, A.; et al. Comparison of satellite-based evapotranspiration models over terrestrial ecosystems in China. *Remote Sens. Environ.* **2014**, *140*, 279–293. [CrossRef]

15. Liaqat, U.W.; Choi, M.; Awan, U.K. Spatio-temporal distribution of actual evapotranspiration in the indus basin irrigation system. *Hydrol. Process.* **2015**, *29*, 2613–2627. [CrossRef]

16. Zeng, R.; Cai, X. Assessing the temporal variance of evapotranspiration considering climate and catchment storage factors. *Adv. Water Resour.* **2015**, *79*, 51–60. [CrossRef]

17. Roderick, M.L.; Farquhar, G.D. The cause of decreased pan evaporation over the past 50 years. *Science* **2002**, *298*, 1410–1411. [PubMed]

18. Gao, G.; Chen, D.; Xu, C.Y.; Simelton, E. Trend of estimated actual evapotranspiration over China during 1960–2002. *J. Geophys. Res. Atmos.* **2007**, *112*, D11120. [CrossRef]

19. Cong, Z.T.; Yang, D.W.; Ni, G.H. Does evaporation paradox exist in China? *Hydrol. Earth Syst. Sci.* **2009**, *13*, 357–366. [CrossRef]

20. Tabari, H.; Marofi, S.; Aeini, A.; Talaee, P.H.; Mohammadi, K. Trend analysis of reference evapotranspiration in the western half of iran. *Agric. For. Meteorol.* **2011**, *151*, 128–136. [CrossRef]

21. Espadafor, M.; Lorite, I.J.; Gavilán, P.; Berengena, J. An analysis of the tendency of reference evapotranspiration estimates and other climate variables during the last 45 years in Southern Spain. *Agric. Water Manag.* **2011**, *98*, 1045–1061. [CrossRef]

22. Łabędzki, L.; Bąk, B.; Smarzyńska, K. Spatio-temporal variability and trends of penman-monteith reference evapotranspiration (fao-56) in 1971–2010 under climatic conditions of Poland. *Pol. J. Environ. Stud.* **2014**, *23*, 2083–2091. [CrossRef]

23. Li, C.; Wu, P.T.; Li, X.L.; Zhou, T.W.; Sun, S.K.; Wang, Y.B.; Luan, X.B.; Yu, X. Spatial and temporal evolution of climatic factors and its impacts on potential evapotranspiration in loess plateau of northern Shaanxi, China. *Sci. Total Environ.* **2017**, *589*, 165–172. [CrossRef] [PubMed]

24. Matin, M.A.; Bourque, C.P.A. Assessing spatiotemporal variation in actual evapotranspiration for semi-arid watersheds in Northwest China: Evaluation of two complementary-based methods. *J. Hydrol.* **2013**, *486*, 455–465. [CrossRef]

25. Zhang, B.; Xu, D.; Liu, Y.; Li, F.; Cai, J.; Du, L. Multi-scale evapotranspiration of summer maize and the controlling meteorological factors in North China. *Agric. For. Meteorol.* **2016**, *216*, 1–12. [CrossRef]

26. Gao, Z.; He, J.; Dong, K.; Li, X. Trends in reference evapotranspiration and their causative factors in the West Liao River Basin, China. *Agric. For. Meteorol.* **2017**, *232*, 106–117. [CrossRef]

27. Wang, Z.; Xie, P.; Lai, C.; Chen, X.; Wu, X.; Zeng, Z.; Li, J. Spatiotemporal variability of reference evapotranspiration and contributing climatic factors in china during 1961–2013. *J. Hydrol.* **2017**, *544*, 97–108. [CrossRef]

28. Gong, L.; Xu, C.-Y.; Chen, D.; Halldin, S.; Chen, Y.D. Sensitivity of the penman–monteith reference evapotranspiration to key climatic variables in the Changjiang (Yangtze River) Basin. *J. Hydrol.* **2006**, *329*, 620–629. [CrossRef]

29. Yang, H.; Yang, D. Climatic factors influencing changing pan evaporation across China from 1961 to 2001. *J. Hydrol.* **2012**, *414–415*, 184–193. [CrossRef]

30. Zhao, L.; Xia, J.; Sobkowiak, L.; Li, Z. Climatic characteristics of reference evapotranspiration in the Hai River Basin and their attribution. *Water (Switz.)* **2014**, *6*, 1482–1499. [CrossRef]

31. Jhajharia, D.; Dinpashoh, Y.; Kahya, E.; Singh, V.P.; Fakheri-Fard, A. Trends in reference evapotranspiration in the humid region of Northeast India. *Hydrol. Process.* **2012**, *26*, 421–435. [CrossRef]

32. McVicar, T.R.; Roderick, M.L.; Donohue, R.J.; Li, L.T.; Van Niel, T.G.; Thomas, A.; Grieser, J.; Jhajharia, D.; Himri, Y.; Mahowald, N.M.; et al. Global review and synthesis of trends in observed terrestrial near-surface wind speeds: Implications for evaporation. *J. Hydrol.* **2012**, *416–417*, 182–205. [CrossRef]

33. Fan, Z.X.; Thomas, A. Spatiotemporal variability of reference evapotranspiration and its contributing climatic factors in Yunnan Province, SW China, 1961–2004. *Clim. Chang.* **2013**, *116*, 309–325. [CrossRef]

34. Choi, M.; Kustas, W.P.; Anderson, M.C.; Allen, R.G.; Li, F.; Kjaersgaard, J.H. An intercomparison of three remote sensing-based surface energy balance algorithms over a corn and soybean production region (iowa, u.S.) during smacex. *Agric. For. Meteorol.* **2009**, *149*, 2082–2097. [CrossRef]

35. Ershadi, A.; McCabe, M.F.; Evans, J.P.; Walker, J.P. Effects of spatial aggregation on the multi-scale estimation of evapotranspiration. *Remote Sens. Environ.* **2013**, *131*, 51–62. [CrossRef]

36. García, M.; Sandholt, I.; Ceccato, P.; Ridler, M.; Mougin, E.; Kergoat, L.; Morillas, L.; Timouk, F.; Fensholt, R.; Domingo, F. Actual evapotranspiration in drylands derived from in-situ and satellite data: Assessing biophysical constraints. *Remote Sens. Environ.* **2013**, *131*, 103–118. [CrossRef]

37. Allen, R.G.; Pereira, L.S.; Howell, T.A.; Jensen, M.E. Evapotranspiration information reporting: II. Recommended documentation. *Agric. Water Manag.* **2011**, *98*, 921–929. [CrossRef]

38. Chu, R.; Li, M.; Shen, S.; Islam, A.R.M.T.; Cao, W.; Tao, S.; Gao, P. Changes in reference evapotranspiration and its contributing factors in Jiangsu, a major economic and agricultural province of Eastern China. *Water (Switz.)* **2017**, *9*, 486. [CrossRef]

39. Tegos, A.; Malamos, N.; Koutsoyiannis, D. A parsimonious regional parametric evapotranspiration model based on a simplification of the penman-monteith formula. *J. Hydrol.* **2015**, *524*, 708–717. [CrossRef]

40. Allan, R.G.; Pereira, L.S.; Raes, D.; Smith, M. *Crop Evapotranspiration: Guidelines for Computing Crop Water Requirements*; Irrigation and Drainage Paper 56; FAO: Rome, Italy, 1998.

41. Bindhu, V.M.; Narasimhan, B.; Sudheer, K.P. Development and verification of a non-linear disaggregation method (nl-distrad) to downscale modis land surface temperature to the spatial scale of landsat thermal data to estimate evapotranspiration. *Remote Sens. Environ.* **2013**, *135*, 118–129. [CrossRef]

42. Mahmoud, S.H.; Alazba, A.A. A coupled remote sensing and the surface energy balance based algorithms to estimate actual evapotranspiration over the western and southern regions of Saudi Arabia. *J. Asian Earth Sci.* **2016**, *124*, 269–283. [CrossRef]

43. Kalma, J.D.; McVicar, T.R.; McCabe, M.F. Estimating land surface evaporation: A review of methods using remotely sensed surface temperature data. *Surv. Geophys.* **2008**, *29*, 421–469. [CrossRef]

44. Yang, G.; Pu, R.; Zhao, C.; Xue, X. Estimating high spatiotemporal resolution evapotranspiration over a winter wheat field using an ikonos image based complementary relationship and lysimeter observations. *Agric. Water Manag.* **2014**, *133*, 34–43. [CrossRef]

45. Bisquert, M.; Sánchez, J.M.; Caselles, V. Evaluation of disaggregation methods for downscaling modis land surface temperature to landsat spatial resolution in barrax test site. *IEEE J. Sel. Top. Appl. Earth Obs. Remote Sens.* **2016**, *9*, 1430–1438. [CrossRef]

46. Jarchow, C.J.; Nagler, P.L.; Glenn, E.P.; Ramírez-Hernandez, J.; Rodríguez-Burgueño, E. Evapotranspiration by remote sensing: An analysis of the colorado river delta before and after the minute 319 pulse flow to mexico. *Ecol. Eng.* **2017**, *106*, 725–732. [CrossRef]

47. Moran, M.S.; Rahman, A.F.; Washburne, J.C.; Goodrich, D.C.; Weltz, M.A.; Kustas, W.P. Combining the penman-monteith equation with measurements of surface temperature and reflectance to estimate evaporation rates of semiarid grassland. *Agric. For. Meteorol.* **1996**, *80*, 87–109. [CrossRef]

48. Bateni, S.M.; Liang, S. Estimating surface energy fluxes using a dual-source data assimilation approach adjoined to the heat diffusion equation. *J. Geophys. Res. Atmos.* **2012**, *117*, D17118. [CrossRef]

49. Mu, Q.; Heinsch, F.A.; Zhao, M.; Running, S.W. Development of a global evapotranspiration algorithm based on modis and global meteorology data. *Remote Sens. Environ.* **2007**, *111*, 519–536. [CrossRef]

50. Mu, Q.; Zhao, M.; Running, S.W. Improvements to a modis global terrestrial evapotranspiration algorithm. *Remote Sens. Environ.* **2011**, *115*, 1781–1800. [CrossRef]

51. Trambauer, P.; Dutra, E.; Maskey, S.; Werner, M.; Pappenberger, F.; Van Beek, L.P.H.; Uhlenbrook, S. Comparison of different evaporation estimates over the african continent. *Hydrol. Earth Syst. Sci.* **2014**, *18*, 193–212. [CrossRef]

52. Autovino, D.; Minacapilli, M.; Provenzano, G. Modelling bulk surface resistance by modis data and assessment of mod16a2 evapotranspiration product in an irrigation district of southern italy. *Agric. Water Manag.* **2016**, *167*, 86–94. [CrossRef]

53. Wambura, F.J.; Dietrich, O.; Lischeid, G. Evaluation of spatio-temporal patterns of remotely sensed evapotranspiration to infer information about hydrological behaviour in a data-scarce region. *Water (Switz.)* **2017**, *9*, 333. [CrossRef]

54. Kim, H.W.; Hwang, K.; Mu, Q.; Lee, S.O.; Choi, M. Validation of modis 16 global terrestrial evapotranspiration products in various climates and land cover types in Asia. *KSCE J. Civ. Eng.* **2012**, *16*, 229–238. [CrossRef]

55. Wu, G.; Liu, Y.; Zhao, X.; Chun, Y.E. Spatio-temporal variations of evapotranspiration in Poyang Lake Basin using mod16 products. *Sci. Geogr. Sin.* **2013**, *33*, 1125–1131.

56. He, T.; Shao, Q. Spatial-temporal variation of terrestrial evapotranspiration in china from 2001 to 2010 using mod16 products. *J. Geo-Inf. Sci.* **2014**, *16*, 979–988.

57. Li, W.; Yi, X.; Cai, D.; Zhang, G.; Liu, S. Analysis of drought characteristics in hainan island based on mod16 evapotranspiration data. *J. Nat. Disasters* **2016**, *25*, 176–183.

58. Zhang, Y.; Chiew, F.H.S.; Zhang, L.; Li, H. Use of remotely sensed actual evapotranspiration to improve rainfall-runoff modeling in southeast australia. *J. Hydrometeorol.* **2009**, *10*, 969–980. [CrossRef]

59. Zhang, Q.; Singh, V.P.; Peng, J.; Chen, Y.D.; Li, J. Spatial–temporal changes of precipitation structure across the Pearl River Basin, China. *J. Hydrol.* **2012**, *440*, 113–122. [CrossRef]

60. Zhang, Q.; Xu, C.Y.; Gemmer, M.; Chen, Y.D.; Liu, C. Changing properties of precipitation concentration in the Pearl River Basin, China. *Stoch. Environ. Res. Risk Assess.* **2009**, *23*, 377–385. [CrossRef]

61. Xiucang, L.; Jiang, T.; Wen, S.S.; Wang, Y.J.; Qiu, X.F. Spatio-temporal variation of actual evapotranspiration and its impact factors in the Pearl River Basin, China. *J. Trop. Meteorol.* **2014**, *30*. [CrossRef]

62. Wang, Z.; Qin, J.; Chen, X. Variation characteristics and impact factors of pan evaporation in Pearl River Basin, China. *Trans. Chin. Soc. Agric. Eng.* **2010**, *26*, 73–77.

63. Chen, Y.D.; Zhang, Q.; Xiao, M.; Singh, V.P.; Zhang, S. Probabilistic forecasting of seasonal droughts in the Pearl River Basin, China. *Stoch. Environ. Res. Risk Assess.* **2016**, *30*, 2031–2040. [CrossRef]

64. Xu, C.Y.; Gong, L.; Jiang, T.; Chen, D.; Singh, V.P. Analysis of spatial distribution and temporal trend of reference evapotranspiration and pan evaporation in Changjiang (Yangtze River) catchment. *J. Hydrol.* **2006**, *327*, 81–93. [CrossRef]

65. Zhang, T.; Peng, J.; Liang, W.; Yang, Y.; Liu, Y. Spatial-temporal patterns of water use efficiency and climate controls in China's loess plateau during 2000–2010. *Sci. Total Environ.* **2016**, *565*, 105–122. [CrossRef] [PubMed]

66. Mann, H.B. Nonparametric tests against trend. *Econometrica* **1945**, *13*, 245–259. [CrossRef]

67. Kendall, M.G. *Rank Correlation Methods*; Griffin: Oxford, UK, 1948.

68. Pearson, K. Note on regression and inheritance in the case of two parents. *Proc. R. Soc. Lond.* **1895**, *58*, 240–242. [CrossRef]

69. You, G.; Zhang, Y.; Liu, Y.; Song, Q.; Lu, Z.; Tan, Z.; Wu, C.; Xie, Y. On the attribution of changing pan evaporation in a nature reserve in SW China. *Hydrol. Process.* **2013**, *27*, 2676–2682. [CrossRef]

70. Niu, J.; Chen, J. A wavelet perspective on variabilities of hydrological processes in conjunction with geomorphic analysis over the Pearl River Basin in South China. *J. Hydrol.* **2016**, *542*, 392–409. [CrossRef]

71. Wang, Z.; Chen, X.; Li, Y. Spatio-temporal changes of ndvi in the Pearl River Basin. *Ecol. Sci.* **2006**, *25*, 303–307.

72. Li, X.; Gemmer, M.; Zhai, J.; Liu, X.; Su, B.; Wang, Y. Spatio-temporal variation of actual evapotranspiration in the Haihe River Basin of the past 50 years. *Quat. Int.* **2013**, *304*, 133–141. [CrossRef]

73. Zeng, L.; Song, K.; Zhang, B.; Wang, Z.; Du, J. Analysis of spatiotemporal variations in evapotranspiration and its influencing factors over the songnen plain in the growing season during the period 2000–2008. *Resour. Sci.* **2010**, *32*, 2305–2315.

74. Wang, P.; Yan, J.; Jiang, C.; Cao, Y. Spatial and temporal variations of evapotranspiration and its influencing factors in the loess plateau in Shaanxi-Gansu-Ningxia Region. *J. Desert Res.* **2016**, *36*, 499–507.

75. Zou, M.; Zhong, L.; Ma, Y.; Hu, Y.; Feng, L. Estimation of actual evapotranspiration in the Nagqu River Basin of the Tibetan Plateau. *Theor. Appl. Climatol.* **2017**, 1–9. [CrossRef]

76. Yin, Y.; Wu, S.; Chen, G.; Dai, E. Attribution analyses of potential evapotranspiration changes in China since the 1960s. *Theor. Appl. Climatol.* **2010**, *101*, 19–28. [CrossRef]

77. Nouri, M.; Homaee, M.; Bannayan, M. Quantitative trend, sensitivity and contribution analyses of reference evapotranspiration in some arid environments under climate change. *Water Resour. Manag.* **2017**, *31*, 2207–2224. [CrossRef]

78. Mosaedi, A.; Ghabaei Sough, M.; Sadeghi, S.H.; Mooshakhian, Y.; Bannayan, M. Sensitivity analysis of monthly reference crop evapotranspiration trends in Iran: A qualitative approach. *Theor. Appl. Climatol.* **2017**, *128*, 857–873. [CrossRef]